

---

This is an electronic reprint of the original article.  
This reprint may differ from the original in pagination and typographic detail.

Prozheeva, V.; Hölldobler, R.; Von Wenckstern, H.; Grundmann, M.; Tuomisto, F.

## Effects of alloy composition and Si-doping on vacancy defect formation in $(\text{In}_x\text{Ga}_{1-x})_2\text{O}_3$ thin films

*Published in:*  
Journal of Applied Physics

*DOI:*  
[10.1063/1.5022245](https://doi.org/10.1063/1.5022245)

Published: 28/03/2018

*Document Version*  
Publisher's PDF, also known as Version of record

*Please cite the original version:*  
Prozheeva, V., Hölldobler, R., Von Wenckstern, H., Grundmann, M., & Tuomisto, F. (2018). Effects of alloy composition and Si-doping on vacancy defect formation in  $(\text{In}_x\text{Ga}_{1-x})_2\text{O}_3$  thin films. *Journal of Applied Physics*, 123(12), 1-6. Article 125705. <https://doi.org/10.1063/1.5022245>

---

This material is protected by copyright and other intellectual property rights, and duplication or sale of all or part of any of the repository collections is not permitted, except that material may be duplicated by you for your research use or educational purposes in electronic or print form. You must obtain permission for any other use. Electronic or print copies may not be offered, whether for sale or otherwise to anyone who is not an authorised user.

## Effects of alloy composition and Si-doping on vacancy defect formation in $(\text{In}_x\text{Ga}_{1-x})_2\text{O}_3$ thin films

V. Prozheeva, R. Hölldobler, H. von Wenckstern, M. Grundmann, and F. Tuomisto

Citation: *Journal of Applied Physics* **123**, 125705 (2018); doi: 10.1063/1.5022245

View online: <https://doi.org/10.1063/1.5022245>

View Table of Contents: <http://aip.scitation.org/toc/jap/123/12>

Published by the *American Institute of Physics*

---

### Articles you may be interested in

[A review of  \$\text{Ga}\_2\text{O}\_3\$  materials, processing, and devices](#)

*Applied Physics Reviews* **5**, 011301 (2018); 10.1063/1.5006941

[Guest Editorial: The dawn of gallium oxide microelectronics](#)

*Applied Physics Letters* **112**, 060401 (2018); 10.1063/1.5017845

[Iron and intrinsic deep level states in  \$\text{Ga}\_2\text{O}\_3\$](#)

*Applied Physics Letters* **112**, 042104 (2018); 10.1063/1.5020134

[On the feasibility of p-type  \$\text{Ga}\_2\text{O}\_3\$](#)

*Applied Physics Letters* **112**, 032108 (2018); 10.1063/1.5009423

[High breakdown voltage quasi-two-dimensional  \$\beta\text{-Ga}\_2\text{O}\_3\$  field-effect transistors with a boron nitride field plate](#)

*Applied Physics Letters* **112**, 122102 (2018); 10.1063/1.5018238

[Compensation and persistent photocapacitance in homoepitaxial Sn-doped  \$\beta\text{-Ga}\_2\text{O}\_3\$](#)

*Journal of Applied Physics* **123**, 115702 (2018); 10.1063/1.5025916

---

Quantum Design Brings You the Next Generation Magneto-Optic Cryostat

Only be limited by your imagination...

Room Temperature Window  
Split-Coil Conical Magnet  
Sample Pod  
User Wiring Ports

Learn More

Quantum Design  
qdusa.com/opticool5

8 Optical Access Ports: 7 Side; 1 Top  
Temperature Range: 1.7 K to 350 K  
7 T Split-Coil Conical Magnet  
Low Vibration: <10 nm peak-to-peak  
89 mm x 84 mm Sample Volume  
Automated Temperature & Magnet Control  
Cryogen Free

# Effects of alloy composition and Si-doping on vacancy defect formation in $(\text{In}_x\text{Ga}_{1-x})_2\text{O}_3$ thin films

V. Prozheeva,<sup>1</sup> R. Hölldobler,<sup>2</sup> H. von Wenckstern,<sup>2</sup> M. Grundmann,<sup>2</sup> and F. Tuomisto<sup>1</sup>

<sup>1</sup>*Department of Applied Physics, Aalto University School of Science, P.O. Box 15100, FI-00076 Aalto, Finland*

<sup>2</sup>*Fakultät für Physik und Geowissenschaften, Universität Leipzig, Felix-Bloch-Institut für Festkörperphysik, Linnéstrasse 5, 04103 Leipzig, Germany*

(Received 12 January 2018; accepted 8 March 2018; published online 29 March 2018)

Various nominally undoped and Si-doped  $(\text{In}_x\text{Ga}_{1-x})_2\text{O}_3$  thin films were grown by pulsed laser deposition in a continuous composition spread mode on *c*-plane  $\alpha$ -sapphire and (100)-oriented MgO substrates. Positron annihilation spectroscopy in the Doppler broadening mode was used as the primary characterisation technique in order to investigate the effect of alloy composition and dopant atoms on the formation of vacancy-type defects. In the undoped samples, we observe a  $\text{Ga}_2\text{O}_3$ -like trend for low indium concentrations changing to  $\text{In}_2\text{O}_3$ -like behaviour along with the increase in the indium fraction. Increasing indium concentration is found to suppress defect formation in the undoped samples at  $[\text{In}] > 70$  at. %. Si doping leads to positron saturation trapping in  $V_{\text{In}}$ -like defects, suggesting a vacancy concentration of at least  $\text{mid-}10^{18} \text{ cm}^{-3}$  independent of the indium content. *Published by AIP Publishing.* <https://doi.org/10.1063/1.5022245>

## I. INTRODUCTION

Major research interest in transparent semiconducting oxides (TSOs) so far has been mostly devoted to binaries. Among them, ZnO remains the indisputable leader of the oxide charts, while  $\text{In}_2\text{O}_3$ ,  $\text{Ga}_2\text{O}_3$ , and  $\text{SnO}_2$  are still intriguing for the researchers.<sup>1</sup> Similar to III-nitrides, alloying  $\text{Ga}_2\text{O}_3$  with  $\text{In}_2\text{O}_3$  or with  $\text{Al}_2\text{O}_3$  permits the bandgap tuning in the wide range of 2.9 eV for  $\text{In}_2\text{O}_3$  to 8.8 eV for  $\alpha$ - $\text{Al}_2\text{O}_3$ .<sup>2,3</sup> Unfortunately, the polymorphism of group-III sesquioxides leads to an increasing complexity of ternary materials and results in slow progress in the field. Clearly, in order to pave the way for competitive and remunerative fabrication of group-III sesquioxide-based devices, a comprehensive study of the compositional dependence on the properties of ternary alloys should be intensified.<sup>4–10</sup> In particular, the experimental studies of  $(\text{In}_x\text{Ga}_{1-x})_2\text{O}_3$  grown by pulsed-laser deposition (PLD) in a continuous composition spread (CCS) mode have shown the efficiency of such an approach for studying the structural and electronic properties of  $(\text{In}_x\text{Ga}_{1-x})_2\text{O}_3$  as a function of indium content.<sup>11–13</sup> In this way, the properties of thin films with the required compositional gradient deposited on 2-in. substrates might be investigated in one flow. The Easter egg of CSS-PLD reveals crystallographic phases such as a hexagonal  $\text{InGaO}_3$  II phase, which would have been missed with the traditional approach of “quantised” sample series preparation.<sup>11,12</sup>

In this paper, we present the results obtained by positron annihilation spectroscopy in thin film  $(\text{In}_x\text{Ga}_{1-x})_2\text{O}_3$  sample series with a graded indium or dopant (silicon) content grown by CCS-PLD on *c*-plane  $\alpha$ -sapphire and (100)-oriented MgO substrates. Vacancy defect formation is discussed in light of alloy composition and doping effects. We show that the increasing indium concentration first enhances the defect formation up to  $x = 0.7$  and then suppresses it for the highest indium content. Si-doping leads to a high vacancy concentration (in the  $\text{mid-}10^{18} \text{ cm}^{-3}$  range).

## II. SAMPLES

A series of  $(\text{In}_x\text{Ga}_{1-x})_2\text{O}_3$  thin films were grown on *c*-plane  $\alpha$ -sapphire (*c*-sapphire in the following) and (100)-oriented MgO by PLD employing segmented targets, allowing lateral continuous composition spread of In in the undoped and Si in the doped samples. All samples were grown under similar conditions at 650–690 °C on 2-in. wafers without any post-treatment with a total pulse count of 50 000 for samples grown on *c*-sapphire and 60 000 pulses for thin films on MgO. Two Si-doped  $(\text{In}_x\text{Ga}_{1-x})_2\text{O}_3$  samples with  $x = 0.3$  and  $0.4$  and with the desirable cation share of 0.5 at. % Si have been produced at  $p_{\text{O}_2} = 8 \times 10^{-2}$  mbar with the aim of increasing the electrical conductivity of the thin films, as has been shown in Ref. 14 for  $\text{Ga}_2\text{O}_3$ . An unintentionally doped sample produced under similar growth conditions has been primarily characterised as a representative of undoped  $(\text{In}_x\text{Ga}_{1-x})_2\text{O}_3$  with 30 and 40 at. % In, corresponding to the Si-doped thin films with a fixed In content. A complementary CCS-PLD  $(\text{In}_x\text{Ga}_{1-x})_2\text{O}_3$  thin film was deposited on (100)-plane MgO in order to investigate potential changes related to a different substrate. Further, another undoped sample has been grown at an oxygen background pressure of  $p_{\text{O}_2} = 3 \times 10^{-4}$  mbar using a two-segmented  $\text{In}_2\text{O}_3/\text{Ga}_2\text{O}_3$  PLD-target. An overview of the basic sample properties is provided in Table I. The details of the growth method and structural characterisation of the undoped samples can be found in Refs. 11, 12, and 15. The thickness of the films was determined using transmission measurements with a Perkin-Elmer Lambda 40 spectrometer and standard spectroscopic ellipsometry applying the Cauchy model.<sup>16</sup> Energy-dispersive X-ray spectroscopy (EDX) and X-ray diffraction (XRD) were used for structural characterisation of the thin films.

Hall measurements in van der Pauw geometry have demonstrated a high free carrier concentration in the range of  $n = 3 \times 10^{19} - 1 \times 10^{20} \text{ cm}^{-3}$  and  $n = 1 \times 10^{19} - 2 \times 10^{19} \text{ cm}^{-3}$  for samples S-40-Si and S-30-Si, respectively. Both doped

TABLE I. Sample thickness  $d$ , In content, and doping levels of the studied samples. In sample S-low- $p$ , the lower thickness corresponds to the Ga-rich side. Thin films S-30-Si and S-40-Si were thicker in the central part of the wafer. All samples except for sample M were grown on  $c$ -sapphire substrates. The dopant fraction refers to the content of the PLD targets used. The oxygen partial pressure  $p_{O_2}$  in the PLD chamber and the substrate temperature  $T$  are indicated.

Sample	$d$ , nm	In content, at. %	Dopant fraction,		$p_{O_2}$ , mbar	$T$ , °C
			at. %			
S-low- $p$	200–700	0.5–80	...		$3 \times 10^{-4}$	650
S	420	0.5–80	...		$8 \times 10^{-2}$	680
S-30-Si	650–700	30	Si, 0.5		$8 \times 10^{-2}$	665
S-40-Si	660–700	40	Si, 0.5		$8 \times 10^{-2}$	661
M	500	10–85	...		$8 \times 10^{-2}$	650

samples were found to have a very low mobility of charge carriers of  $1\text{--}4\text{ cm}^2/\text{Vs}$ , as typically reported for heteroepitaxial  $\text{Ga}_2\text{O}_3$  thin films.<sup>14</sup> The undoped sample S-low- $p$  was highly resistive, except for the region with  $[\text{In}] > 25$  at. %, where the free carrier concentration increased up to  $n = 1 \times 10^{17}\text{--}1 \times 10^{18}\text{ cm}^{-3}$ .

### A. EDX

The spatial variation of the chemical composition of thin films was investigated by EDX using a field-emission scanning electron microscope FEI NovaLab 200 equipped with an Ametek EDAX detector. The shape of the EDX line scan for the undoped sample S-low- $p$  is discussed in detail in Ref. 12. The undoped samples S and M have linear or slightly S-shaped variation of the In content along the compositional gradient, as shown in Fig. 1. The In content of both Si-doped samples is essentially constant all over the thin films: 29–30 at. % for S-30-Si and 39–40 at. % for S-40-Si.

The incorporation of indium is strongly dependent on the oxygen background pressure. For the sample grown at low  $p_{O_2}$ , the indium incorporation is clearly below expectations from Monte-Carlo (MC) simulations.<sup>15</sup> For samples grown at high  $p_{O_2}$ , the incorporation of indium corresponds to the results of the MC simulations. This is likely due to the higher bonding strength of the Ga-O bond with respect to In-O and is similar to the results reported for group-III nitrides.<sup>17,18</sup>

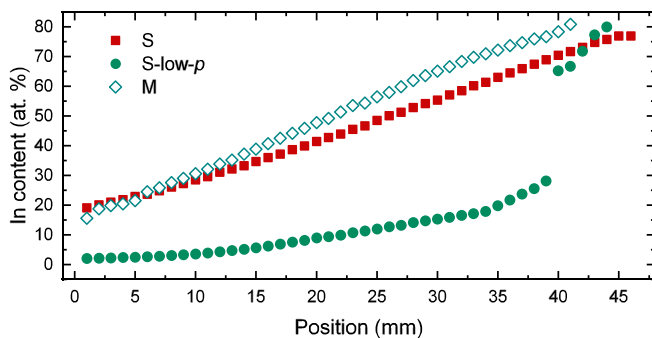


FIG. 1. Line scans of the In content along the compositional gradient in selected samples as determined by EDX measurements.

### B. XRD

Spatially resolved XRD measurements were conducted on a PANalytical X'pert PRO MRD diffractometer and a PIXcel3D detector in the 1D scanning mode. The example XRD patterns for the Si-doped thin film and for the undoped sample with a linear In gradient are presented in Fig. 2. In each case, 55  $2\theta - \omega$  scans were recorded with a 1 mm step along the compositional gradient.

Both Si-doped samples were found to crystallise in hex-InGaO<sub>3</sub> II, irrespective of the dopant content. In sample S, the (222) bcc-In<sub>2</sub>O<sub>3</sub> reflection is clearly observed at  $[\text{In}] > 70$  at. %, followed by a side phase seen at lower angles between 30 and 70 at. % In, which might be attributed to the (004)-plane of the hexagonal InGaO<sub>3</sub> II phase. At the low indium content,  $[\text{In}] < 30$  at. %, a shift in the peak position towards higher angles is observed. An overview of the crystallographic phases present in the studied samples is presented in Table II.

### III. POSITRON ANNIHILATION SPECTROSCOPY

#### A. Experimental details

The evolution of vacancy-type defects as a function of the alloy and dopant compositions was monitored using positron annihilation spectroscopy in the Doppler broadening mode. The Doppler broadening of the 511 keV annihilation line is mostly caused by the momentum of the annihilating electrons. The lineshape of the annihilation peak is wider when a positron is in a delocalized state and narrower when it is trapped in a vacancy-type defect due to the reduced overlap of the positron wavefunction with core electron wavefunctions. The atoms surrounding the annihilation site also have an impact on the obtained signal.<sup>19</sup>

The thin films were studied using a variable energy positron beam. By controlling the implantation energy and, consequently, the kinetic energy of positrons, the probing depth is varied from the surface up to 2  $\mu\text{m}$ . After implantation, the positron thermalizes in the sample within a few picoseconds and diffuses for 100–250 ps (100–200 nm depending on the material and the crystalline quality) before annihilating with an electron. The resolution of the HPGe detector used for measuring the Doppler broadening of the annihilation line was 1.2 keV at 511 keV. The peak lineshape was analysed using conventional low momentum parameter  $S$  corresponding to longitudinal electron momenta at  $[-0.4\text{--}0.4]$  a.u., and the  $\pm[1.6\text{--}4.0]$  a.u. window was applied for the high momentum  $W$  parameter. The  $S$  parameter reflects the open volume of a vacancy, and the  $W$  parameter is sensitive to the immediate surroundings of the vacancy being representative of positron annihilations with core electrons. For further details on the measurement technique, see Ref. 19. The Doppler broadening parameters were measured as a function of positron implantation energy and, hence, the probing depth, along the compositional gradient in CCS thin films with a step of 2–10 mm depending on the sample. Reference measurements were performed in earlier-characterised single crystal bulk In<sub>2</sub>O<sub>3</sub> (Ref. 20), giving  $S_{\text{ref}} = 0.44(6)$  and  $W_{\text{ref}}$

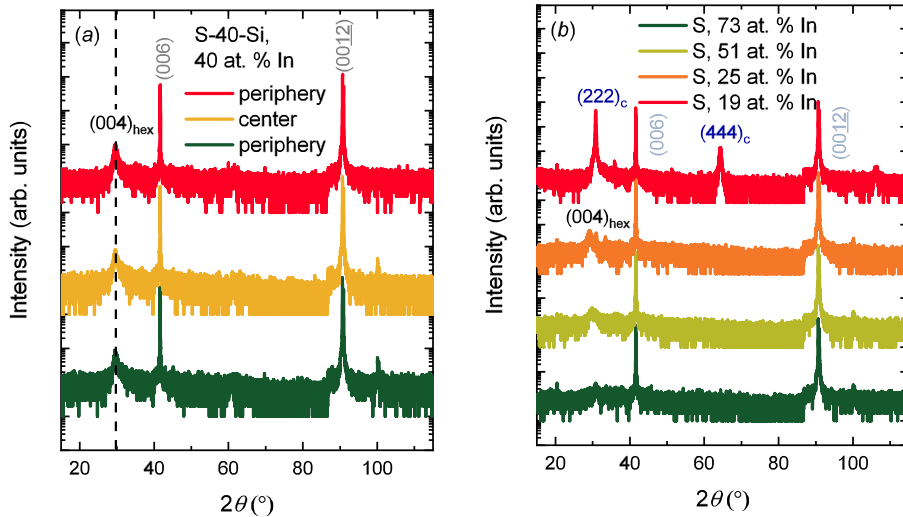


FIG. 2. (a) The individual XRD patterns from the wide-angle  $2\theta - \omega$  scans for the Si-doped  $(\text{In}_{0.4}\text{Ga}_{0.3})_2\text{O}_3$  thin film S-40-Si along the wafer. (b) The individual XRD patterns from the wide-angle  $2\theta - \omega$  scans for the undoped sample S along the In gradient. The subscript “c” refers to bcc- $\text{In}_2\text{O}_3$ . The subscript “hex” refers to the hexagonal  $\text{InGaO}_3$  II phase. The substrate-related peaks are marked as (006) and (0012).

$= 0.048(5)$ , and homoepitaxial thin film  $\text{Ga}_2\text{O}_3$  (Ref. 21), giving  $S_{\text{ref}} = 0.43(5)$  and  $W_{\text{ref}} = 0.053(6)$ .

## B. Results and analysis

Figure 3 shows the  $S$  parameter measured as a function of positron implantation energy (implantation depth) for selected alloy compositions in the undoped and Si-doped samples both grown at  $p_{\text{O}_2} = 8 \times 10^{-2}$  mbar on  $c$ -sapphire. The data at low energies ( $< 3$  keV) are dominated by annihilations at the surface due to the diffusion of thermalized positrons back to the surface. The layer of interest is observed between 3 and 9 keV depending on the measurement point.

The  $S(E)$  curve for the sample with a non-linear indium gradient S-low- $p$  in Fig. 4 (left) reveals a similar behaviour. However, the layer-specific  $S$  parameter of sample S-low- $p$  is observed at 3–6 keV for the In-poor side. The thickness of the studied layer slightly increases for the point of 28 at. % In and doubles on the In-rich side, in agreement with structural information provided in Table I and in Ref. 12. At higher energies, positrons start reaching the substrate, and the data for all the samples from the  $S^*$ -series converge to

the value typical for the  $c$ -sapphire substrate at implantation energy  $E > 19$  keV. A fraction of positrons still annihilates in the thicker layer of the In-rich area of sample S-low- $p$  even at  $E > 24$  keV due to the wider positron implantation profile at high implantation energies. The change in the substrate [cf. Fig. 4 (right)] results in the data points converging to a different point at  $E > 20$  keV. Notably, the  $S$  parameter of the Si-doped samples does not differ from one measurement point to another along the dopant gradient and is higher than that of the undoped samples irrespective of the dopant content. In samples S and M, the highest  $S$  parameter is observed at the medium In content and decreases on In-rich as well as on Ga-rich sides. This trend is more strongly pronounced in the sample grown on MgO (sample M). Overall, the  $S$  ( $W$ , not shown) parameter of the studied thin films is higher (lower) than that of the reference  $\text{In}_2\text{O}_3$  and bulk  $\text{Ga}_2\text{O}_3$ , indicating the presence of vacancies in  $(\text{In}_x\text{Ga}_{1-x})_2\text{O}_3$  layers.<sup>20,21</sup>

TABLE II. The crystallographic phases present in the studied samples depending on the In content. The structural properties of samples S-low- $p$  and M were defined in Refs. 11 and 12. The regions are referred to as the following: “mcl” stands for monoclinic  $\beta$ - $\text{Ga}_2\text{O}_3$  and “bcc” and “hex” are for cubic bixbyite  $\text{In}_2\text{O}_3$  and hexagonal  $\text{InGaO}_3$  II, respectively.

Sample	In content, at. %	Crystallographic phases
	$< 20$	mcl
S-low- $p$	20–80	mcl, bcc, hex
	$> 80$	bcc (dominant), hex
	$< 30$	bcc
S	30–70	hex, bcc
	$> 70$	bcc
S-30-Si	30	hex
S-40-Si	40	hex
	$< 30$	mcl
M	40–65	Amorphous region
	$> 65$	bcc

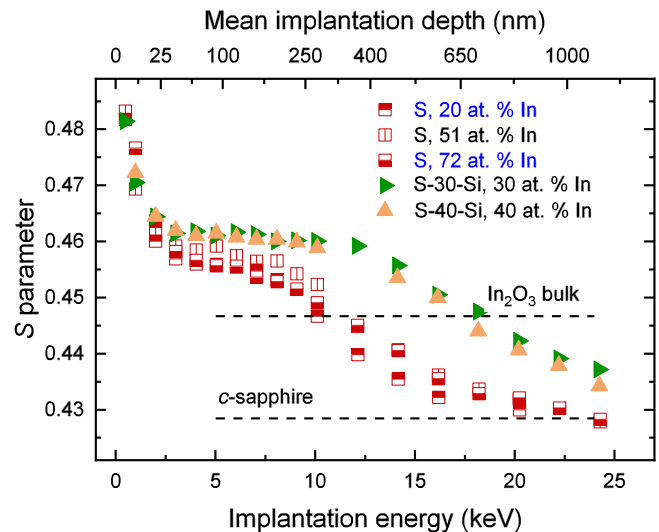


FIG. 3. The  $S$  parameter as a function of positron implantation energy and mean implantation depth corresponding to the undoped sample S and the Si-doped samples S-30-Si and S-40-Si, all on  $c$ -plane sapphire. The colour of the legend text indicates the crystal structure: blue stands for cubic bixbyite  $\text{In}_2\text{O}_3$  and black is for hexagonal  $\text{InGaO}_3$  II or a mixed phase.

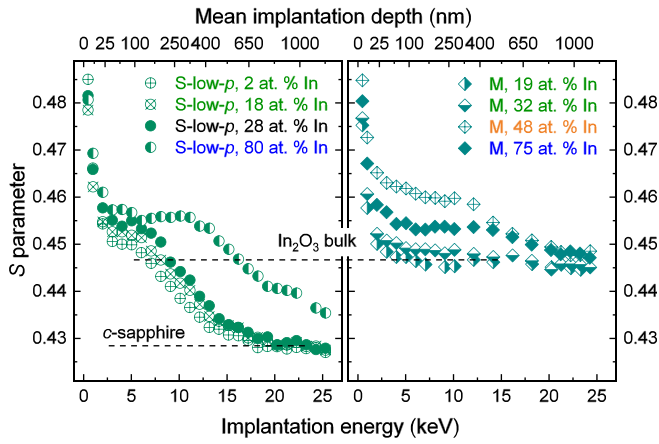


FIG. 4. The  $S$  parameter as a function of positron implantation energy and mean implantation depth corresponding to undoped samples S-low- $p$  on  $c$ -plane sapphire (left) and M on MgO (right). The colour of the legend text indicates the crystal structure: green for monoclinic  $\beta$ - $\text{Ga}_2\text{O}_3$ , blue for cubic bixbyite  $\text{In}_2\text{O}_3$ , black for hexagonal  $\text{InGaO}_3$  II or a mixed phase, and orange for the amorphous region.

Figure 5 presents the layer-specific  $S$  parameter as a function of the compositional gradient in the undoped samples. The increase in the  $S$  parameter observed on the high [In] side of sample S-low- $p$ , see Fig. 5(a), correlates with the phase separation revealed above 60 at. % In.<sup>11,12</sup> For the thin film S, grown at high  $p_{\text{O}_2}$ , the changes in the  $S$  parameter displayed in Fig. 5(b) have a narrower span and demonstrate a tendency to expanding the open volume up to  $\approx 70$  at. % In corresponding to the bcc- $\text{In}_2\text{O}_3$  phase observed in the XRD data. A sharp increase in the  $S$  parameter at an In content of 40 at. % of sample M is shown in Fig. 5(c). One more, although less sharp, change in the  $S$  parameter takes place as the indium content reaches 65 at. %. Such a change in the  $S$  parameter might be attributed to either an increase in the vacancy content or a phase change. The results seem to agree with the phase change scenario, as the sample was found to be monoclinic only up to 30 at. % In, see Table II and Ref. 12.

The qualitative and quantitative characterisation of the vacancy-type positron traps can be performed with the  $(S, W)$  plots shown in Figs. 6(a)–6(c). The layer-specific data presented in the plots were determined as average  $(S, W)$  values in the energy range of 3–10 keV, slightly varying depending on the layer thickness for each measurement point.

The data points for sample S-low- $p$  at relatively low In concentrations ( $< 30$  at. %) fall on a straight line between

$V_{\text{Ga}}$ -like defects (in MOCVD  $\text{Ga}_2\text{O}_3$ , see Ref. 21) and  $\text{Ga}_2\text{O}_3$  bulk. The positron signal evolves with the increasing In content: the  $W$  parameter decreases and the  $S$  parameter increases until the last measured point at 80 at. % In which exhibits a shift to higher  $S$  values. The linear dependence between the  $S$  and  $W$  parameters generally indicates the presence of a single type of vacancy at different concentrations.<sup>19</sup> It should be noted that the multicomponent character of systems such as ternary alloys considered here complicates the data analysis and limits the defect identification to the terms of group-III vacancies. Nevertheless, when progressing along the In gradient from the Ga-rich to In-rich region, the data points move in the direction of increasing defect concentration instead of approaching  $\text{In}_2\text{O}_3$  bulk values.

The positron signal changes for the samples grown at high  $p_{\text{O}_2}$ . The  $(S, W)$  points for sample S [see Fig. 6(b)] are found close to the  $V_{\text{In}}$  defect line. Both samples S-30-Si and S-40-Si have higher  $S$  and lower  $W$  parameters than the corresponding reference points at 20–44 at. % In in the undoped sample S irrespective of the Si-doping level, indicating an increase in the cation vacancy concentration. Figure 6(c) shows the  $(S, W)$  values for selected (In, Ga) compositions in sample M. The points for [In]  $< 40$  at. % follow the  $\text{Ga}_2\text{O}_3 - V_{\text{Ga}}$  line with a trend toward  $V_{\text{Ga}}$  with the increasing In content. At an intermediate In content of 40–65 at. %, the  $(S, W)$  data are clustered close to the same point as for the Si-doped samples. With a further increase in the In content, the data show a trend towards the  $\text{In}_2\text{O}_3$  bulk values.

## IV. DISCUSSION

### A. Alloy composition

We observe a correlation between the cation vacancy content and the increasing In content in the undoped thin films as shown in Fig. 6. Sample S-low- $p$  is reported in Ref. 12 to be monoclinic up to 20 at. % In, and In is fully incorporated into the  $\text{Ga}_2\text{O}_3$  lattice. The point measured at 80 at. % In corresponds to a mixed phase including the hexagonal  $\text{InGaO}_3$  II phase and the dominant bcc- $\text{In}_2\text{O}_3$  phase. Thus, if we omit the last point as being representative of a different phase, the vacancy concentration on the Ga-rich side of sample S-low- $p$  can be estimated to be on the order of  $(2-4) \times 10^{16} \text{ cm}^{-3}$ , increasing with the higher In content, assuming  $\text{Ga}_2\text{O}_3$ -like behaviour and positron trapping in the  $V_{\text{Ga}}$ -type defects.<sup>19</sup> In the case of  $V_{\text{Ga}}$ -like behaviour in

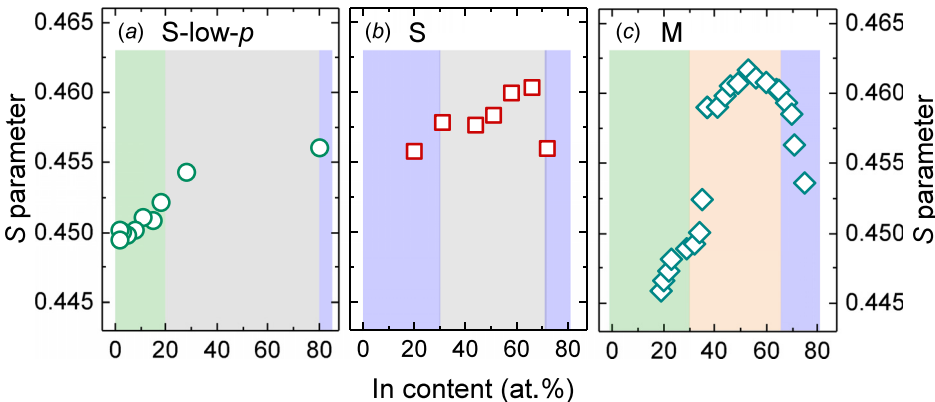


FIG. 5. The  $S$  parameter as a function of In gradient for the undoped samples S-low- $p$  (a), S (b), and M (c). The colour of the background indicates the crystal structure: green for monoclinic  $\beta$ - $\text{Ga}_2\text{O}_3$ , blue for cubic bixbyite  $\text{In}_2\text{O}_3$ , grey for hexagonal  $\text{InGaO}_3$  II or a mixed phase, and orange for the amorphous region.

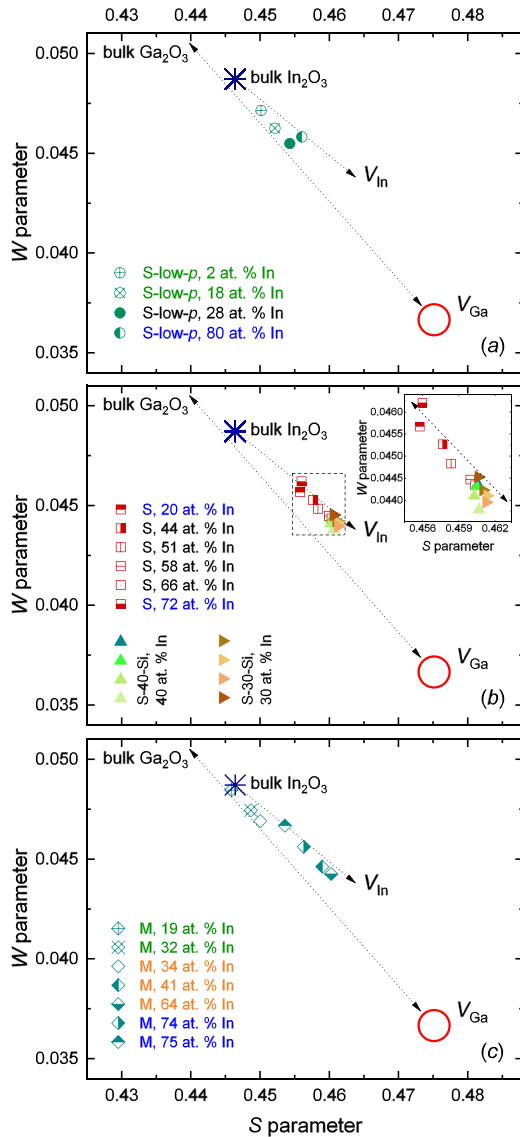


FIG. 6. The  $(S, W)$  parameter plots for (a) undoped sample S-low- $p$ , (b) undoped sample S and Si-doped samples S-30-Si and S-40-Si, all four on  $c$ -plane sapphire, and (c) the undoped sample M grown on  $a$ -plane MgO. Each measurement point is representative of a layer at the selected In content. The values characteristic of bulk  $\text{In}_2\text{O}_3$  are shown for reference. Inset in (b): a closer view to the  $(S, W)$  region representing the  $(\text{In}_x\text{Ga}_{1-x})_2\text{O}_3$  layers. The colour of the legend text indicates the crystal structure: green for monoclinic  $\beta\text{-Ga}_2\text{O}_3$ , blue for cubic bixbyite  $\text{In}_2\text{O}_3$ , black for hexagonal  $\text{InGaO}_3$  II or a mixed phase, and orange for the amorphous region. The dashed lines illustrate the expected  $V_{\text{Ga}}$  and  $V_{\text{In}}$  trends observed earlier.<sup>20,21</sup> The red circles demonstrate the  $(S, W)$  span for  $V_{\text{Ga}}$ -like defects in  $\text{Ga}_2\text{O}_3$ . The error margins are of the size of the data point markers.

sample M, the vacancy concentration at a low In content can be estimated to be  $(1-2) \times 10^{16} \text{ cm}^{-3}$ , slightly less than that in the sample S-low- $p$ . This observation suggests improved crystallinity for growth on MgO substrates for the In content up to 30–40 at. %.

The nature of vacancies in sample S-low- $p$  grown on  $c$ -sapphire tends to  $V_{\text{In}}$ -like at 28 at. % In and in sample M grown on the MgO substrate at 40 at. % In. Assuming that at the high In content, the obtained positron signal is comparable to that of  $V_{\text{In}}$  and the  $\text{In}_2\text{O}_3$ -like lattice, the cation vacancy defect concentration in the sample with non-linear

In gradient S-low- $p$  is in low- to mid- $10^{17} \text{ cm}^{-3}$  range. The step-like shift of the data points to the  $\text{In}_2\text{O}_3$ - $V_{\text{In}}$  line in the  $(S, W)$  plane implies that the  $\text{In}_2\text{O}_3$ -like component prevails over the  $\text{Ga}_2\text{O}_3$ -resembling counterpart in the In-rich region in Figs. 6(a) and 6(c), as expected from the phase change observed in the XRD data. For the sample with a linear In gradient S, Fig. 6(b), the positron signal demonstrates  $\text{In}_2\text{O}_3$ -like nature for all measured points already at 20 at. % In. This observation is in line with the fact that the monoclinic  $\beta\text{-Ga}_2\text{O}_3$  phase was not observed at all for this sample. Among the undoped samples, the highest  $S$  parameter and, subsequently, the highest amount of open volume are observed in samples S and M at a medium indium content corresponding to the mixed phase of decreased crystalline quality including the  $\text{InGaO}_3$  II phase demonstrated in Sec. II B and in Ref. 12. It should be noted that similar evolution of the positron signature might be induced by adding more oxygen vacancies next to the initial cation vacancies. Positively charged isolated oxygen vacancies  $V_{\text{O}}$  are undetectable by positrons and play a role only when cation-anion vacancy complexes are present.<sup>22</sup> However, as the changes are clearly correlated with the phase behaviour of the  $(\text{In}_x\text{Ga}_{1-x})_2\text{O}_3$  alloys, we consider the changes in vacancy complexes to be less likely an explanation for our observations.

The shift towards  $\text{In}_2\text{O}_3$  bulk in Figs. 6(a) and 6(c) for the points measured at  $[\text{In}] > 70$  at. % indicates suppressed  $V_{\text{In}}$ -like group-III vacancy formation along with the appearance of the bcc- $\text{In}_2\text{O}_3$  phase [see Fig. 2(b) and Ref. 12]. These findings are in line with the low formation energy of  $V_{\text{Ga}}$  in  $\text{Ga}_2\text{O}_3$  compared to the vacancy formation energy in  $\text{In}_2\text{O}_3$  which is too high for  $V_{\text{In}}$  to emerge in substantial concentrations.<sup>23</sup> Our earlier experiments in binary oxides also demonstrate that  $V_{\text{In}}$  is much less abundant in  $\text{In}_2\text{O}_3$  than  $V_{\text{Ga}}$  in  $\text{Ga}_2\text{O}_3$ .<sup>20,21</sup>

## B. Doping effects

In the undoped samples, adding In to  $\text{Ga}_2\text{O}_3$  might be viewed as  $n$ -type doping, as  $\text{In}_2\text{O}_3$  tends to be highly conducting, while the conductivity of  $\text{Ga}_2\text{O}_3$  is typically limited.<sup>24,25</sup> This appears to enhance the formation of  $V_{\text{Ga}}$ -like group-III vacancy type defects in the layers for low and sub-medium In contents. Sample M has a lower vacancy concentration than sample S-low- $p$  in the considered region (up to 35 at. % In), probably due to different substrates resulting in higher crystalline quality. We observe  $V_{\text{Ga}}$  concentrations in the low- $10^{16} \text{ cm}^{-3}$  range on the Ga-rich side of the undoped sample S-low- $p$  grown by CCS-PLD, while they have been found to fully compensate for  $n$ -type doping in  $\text{Ga}_2\text{O}_3$  grown by metal-organic chemical vapour deposition.<sup>21</sup> On the other hand, in the predominately cubic In-rich CCS-PLD- $(\text{In}_x\text{Ga}_{1-x})_2\text{O}_3$ , the  $V_{\text{In}}$ -like cation vacancy concentrations are clearly higher ( $\sim 10^{17} \text{ cm}^{-3}$ ), but in  $\text{In}_2\text{O}_3$  grown by molecular beam epitaxy, these defects have been found to be unimportant for electrical compensation.<sup>20</sup>

Comparing the  $(S, W)$  values for the bulk reference  $\text{In}_2\text{O}_3$  and the data points in Fig. 6 at medium In concentrations in undoped samples M and S and in both Si-doped samples, the estimated defect parameters are  $S_{\text{defect}} \geq 1.03 \times S_{\text{bulk}}$  and

$W_{\text{defect}} \leq 0.91 \times W_{\text{bulk}}$ . This span agrees well with the experimental values obtained for Mg- and Sn-doped  $\text{In}_2\text{O}_3$  and with theoretical calculations for  $V_{\text{In}}$  in  $\text{In}_2\text{O}_3$ .<sup>20,22</sup> Assuming that the  $(S,W)$  values for the Si-doped samples represent the state where all positrons are trapped to vacancies, the saturation trapping conditions imply that the  $V_{\text{In}}$  concentration in samples S-30-Si and S-40-Si is at least mid- $10^{18} \text{ cm}^{-3}$  irrespective of the doping level. Doping with Si has been found to substantially increase the vacancy concentration in the binary thin-film  $\text{Ga}_2\text{O}_3$  as well.<sup>21</sup>

## V. SUMMARY

The effect of alloy composition and Si doping on vacancy defect formation in CCS-PLD-grown  $(\text{In}_x\text{Ga}_{1-x})_2\text{O}_3$  thin films was investigated by positron annihilation spectroscopy. Considering the undoped samples, alloying  $\text{Ga}_2\text{O}_3$  with indium in low-to-moderate concentrations (up to 40–60 at. % In) enhances the formation of cation vacancy-type defects. The positron data evolve first demonstrating  $\text{Ga}_2\text{O}_3$ -like behaviour to the  $\text{In}_2\text{O}_3$ -like state at 28 at. % In or at 40 at. % In depending on the substrate. This change is interpreted as reflecting the structural changes such as the formation of hexagonal phase  $\text{InGaO}_3$  II. At the highest indium content (>70 at. % In), the bcc- $\text{In}_2\text{O}_3$  phase is observed in the XRD measurements, and the suppressed defect formation reported here matches the findings for binary  $\text{In}_2\text{O}_3$ .<sup>20</sup> The data for the Si-doped samples suggest saturation trapping in  $V_{\text{In}}$ -like defects, irrespective of the doping level, meaning a substantial defect concentration of at least mid- $10^{18} \text{ cm}^{-3}$ . Our findings illustrate the delicate balance between phenomena governing the defect formation in thin-film growth.

## ACKNOWLEDGMENTS

We would like to thank M. Hahn for preparation of the PLD targets, H. Hochmuth for thin film growth, J. Lenzner for EDX measurements, M. Lorenz for help with XRD measurements, and C. Sturm for the comments on ellipsometry results. This work was supported by European Social Fund within the project “Combinatorisches Oxid-Screening für Materialien und Anwendungen (COSIMA)” (SAB 100282338) and by the Academy of Finland Grant No. 277193.

<sup>1</sup>H. von Wenckstern, “Group-III sesquioxides: Growth, physical properties and devices,” *Adv. Electron. Mater.* **3**, 1600350 (2017).

<sup>2</sup>A. Walsh, J. L. F. Da Silva, S.-H. Wei, C. Körber, A. Klein, L. F. J. Piper, A. DeMasi, K. E. Smith, G. Panaccione, P. Torelli, D. J. Payne, A. Bourlange, and R. G. Egdell, “Nature of the band gap of  $\text{In}_2\text{O}_3$  revealed by first-principles calculations and X-ray spectroscopy,” *Phys. Rev. Lett.* **100**, 167402 (2008).

<sup>3</sup>J. Robertson, “Band offsets of wide-band-gap oxides and implications for future electronic devices,” *J. Vac. Sci. Technol. B* **18**, 1785–1791 (2000).

<sup>4</sup>S. Fujita and K. Kaneko, “Epitaxial growth of corundum-structured wide band gap III-oxide semiconductor thin films,” *J. Cryst. Growth* **401**, 588–592 (2014).

<sup>5</sup>T. Oshima and S. Fujita, “Properties of  $\text{Ga}_2\text{O}_3$ -based  $(\text{In}_x\text{Ga}_{1-x})_2\text{O}_3$  alloy thin films grown by molecular beam epitaxy,” *Phys. Status Solidi C* **5**, 3113–3115 (2008).

<sup>6</sup>F. Yang, J. Ma, C. Luan, and L. Kong, “Structural and optical properties of  $\text{Ga}_{2(1-x)}\text{In}_{2x}\text{O}_3$  films prepared on  $\alpha$ - $(\text{AlGa})_2\text{O}_3$  (0 0 0 1) by MOCVD,” *Appl. Surf. Sci.* **255**, 4401–4404 (2009).

<sup>7</sup>P. Vogt and O. Bierwagen, “Kinetics versus thermodynamics of the metal incorporation in molecular beam epitaxy of  $(\text{In}_x\text{Ga}_{1-x})_2\text{O}_3$ ,” *APL Mater.* **4**, 086112 (2016).

<sup>8</sup>H. Ito, K. Kaneko, and S. Fujita, “Growth and band gap control of corundum-structured  $\alpha$ - $(\text{AlGa})_2\text{O}_3$  thin films on sapphire by spray-assisted mist chemical vapor deposition,” *Jpn. J. Appl. Phys.* **51**, 100207 (2012).

<sup>9</sup>F. Zhang, K. Saito, T. Tanaka, M. Nishio, and Q. Guo, “Wide bandgap engineering of  $(\text{GaIn})_2\text{O}_3$  films,” *Solid State Commun.* **186**, 28–31 (2014).

<sup>10</sup>F. Zhang, K. Saito, T. Tanaka, M. Nishio, M. Arita, and Q. Guo, “Wide bandgap engineering of  $(\text{AlGa})_2\text{O}_3$  films,” *Appl. Phys. Lett.* **105**, 162107 (2014).

<sup>11</sup>H. von Wenckstern, D. Splith, M. Purfürst, Z. Zhang, C. Kranert, S. Müller, M. Lorenz, and M. Grundmann, “Structural and optical properties of  $(\text{In,Ga})_2\text{O}_3$  thin films and characteristics of Schottky contacts thereon,” *Semicond. Sci. Technol.* **30**, 024005 (2015).

<sup>12</sup>C. Kranert, J. Lenzner, M. Jenderka, M. Lorenz, H. von Wenckstern, R. Schmidt-Grund, and M. Grundmann, “Lattice parameters and Raman-active phonon modes of  $(\text{In}_x\text{Ga}_{1-x})_2\text{O}_3$  for  $x < 0.4$ ,” *J. Appl. Phys.* **116**, 013505 (2014).

<sup>13</sup>R. Schmidt-Grund, C. Kranert, T. Böntgen, H. von Wenckstern, H. Krauß, and M. Grundmann, “Dielectric function in the NIR-VUV spectral range of  $(\text{In}_x\text{Ga}_{1-x})_2\text{O}_3$  thin films,” *J. Appl. Phys.* **116**, 053510 (2014).

<sup>14</sup>S. Müller, H. von Wenckstern, D. Splith, F. Schmidt, and M. Grundmann, “Control of the conductivity of Si-doped  $\beta$ - $\text{Ga}_2\text{O}_3$  thin films via growth temperature and pressure,” *Phys. Status Solidi A* **211**, 34–39 (2014).

<sup>15</sup>H. von Wenckstern, Z. Zhang, F. Schmidt, J. Lenzner, H. Hochmuth, and M. Grundmann, “Continuous composition spread using pulsed-laser deposition with a single segmented target,” *CrystEngComm* **15**, 10020–10027 (2013).

<sup>16</sup>H. Fujiwara, *Spectroscopic Ellipsometry: Principles and Applications* (John Wiley and Sons, 2007).

<sup>17</sup>Y. Kangawa, T. Ito, Y. Kumagai, and A. Koukitsu, “Thermodynamic study on compositional instability of  $\text{InGaIn}/\text{GaIn}$  and  $\text{InGaIn}/\text{InN}$  during MBE,” *Appl. Surf. Sci.* **216**, 453–457 (2003).

<sup>18</sup>E. Monroy, N. Gogneau, F. Enjalbert, F. Fossard, D. Jalabert, E. Bellet-Amalric, L. S. Dang, and B. Daudin, “Molecular-beam epitaxial growth and characterization of quaternary III-nitride compounds,” *J. Appl. Phys.* **94**, 3121–3127 (2003).

<sup>19</sup>F. Tuomisto and I. Makkonen, “Defect identification in semiconductors with positron annihilation: Experiment and theory,” *Rev. Mod. Phys.* **85**, 1583–1631 (2013).

<sup>20</sup>E. Korhonen, F. Tuomisto, O. Bierwagen, J. S. Speck, and Z. Galazka, “Compensating vacancy defects in Sn- and Mg-doped  $\text{In}_2\text{O}_3$ ,” *Phys. Rev. B* **90**, 245307 (2014).

<sup>21</sup>E. Korhonen, F. Tuomisto, D. Gogova, G. Wagner, M. Baldini, Z. Galazka, R. Schewski, and M. Albrecht, “Electrical compensation by Ga vacancies in  $\text{Ga}_2\text{O}_3$  thin films,” *Appl. Phys. Lett.* **106**, 242103 (2015).

<sup>22</sup>I. Makkonen, E. Korhonen, V. Prozhheeva, and F. Tuomisto, “Identification of vacancy defect complexes in transparent semiconducting oxides  $\text{ZnO}$ ,  $\text{In}_2\text{O}_3$  and  $\text{SnO}_2$ ,” *J. Phys.: Condens. Matter* **28**, 224002 (2016).

<sup>23</sup>J. B. Varley, H. Peelaers, A. Janotti, and C. G. V. de Walle, “Hydrogenated cation vacancies in semiconducting oxides,” *J. Phys.: Condens. Matter* **23**, 334212 (2011).

<sup>24</sup>O. Bierwagen and J. S. Speck, “Plasma-assisted molecular beam epitaxy of Sn-doped  $\text{In}_2\text{O}_3$ : Sn incorporation, structural changes, doping limits, and compensation,” *Phys. Status Solidi A* **211**, 48–53 (2014).

<sup>25</sup>M. Baldini, M. Albrecht, A. Fiedler, K. Irmischer, D. Klimm, R. Schewski, and G. Wagner, “Semiconducting Sn-doped  $\beta$ - $\text{Ga}_2\text{O}_3$  homoepitaxial layers grown by metal organic vapour-phase epitaxy,” *J. Mater. Sci.* **51**, 3650–3656 (2016).